Supplement of Atmos. Chem. Phys., 24, 12409–12423, 2024
https://doi.org/10.5194/acp-24-12409-2024-supplement

Atmospheric Chemistry and Physics
Open Access
EGU

Supplement of

Rapid oxidation of phenolic compounds by O_3 and $HO^{\bullet}$: effects of the air–water interface and mineral dust in tropospheric chemical processes

Yanru Huo et al.

Correspondence to: Maoxia He (hemaox@sdu.edu.cn)

Table S1. Gibbs free energy of activation ($\Delta G^{\ddagger}$) for the O_3-initiated reaction of Ph, 4-HBA, and VL. Unit: kcal mol $^{-1}$.

Compounds	C1 – C2	C2 – C3	C3 – C4	C4 – C5	C5 – C6	C6 – C1
			Gas-phase			
Ph	19.03	20.60	20.46	–	–	–
4-HBA	23.59	24.22	24.84	24.33	23.47	24.52
VL	22.54	24.46	21.00	25.95	22.51	23.22
			Bulk water			
Ph	14.94	17.88	15.75			
4-HBA	20.21	21.27	22.38	20.92	19.84	20.81
VL	19.17	20.89	17.89	24.43	18.56	19.56
			A-W interface			
Ph	15.18	18.10	12.86			
4-HBA	21.76	22.03	24.69	25.24	23.88	22.36
VL	14.15	19.16	16.01	21.41	21.02	19.81
			TiO_2 clusters			
Ph	25.34	24.46	24.30			
4-HBA	25.91	23.51	23.96	26.53	23.23	27.83
VL	15.98	11.42	17.44	11.14	13.37	14.65

Table S2. Gibbs free energy of reaction ($\Delta_r G$) for the O_3-initiated reaction of Ph, 4-HBA, and VL. Unit: kcal mol $^{-1}$.

Compounds	C1 – C2	C2 – C3	C3 – C4	C4 – C5	C5 – C6	C6 – C1
			Gas-phase			
Ph	-28.85	-25.44	-24.77			
4-HBA	-24.26	-21.71	-17.86	-16.21	-22.74	-21.46
VL	-23.72	-19.55	-20.42	-14.57	-24.02	-26.62
			Bulk water			
Ph	-31.58	-27.21	-30.11			
4-HBA	-26.18	-23.81	-20.32	-19.72	-28.56	-24.50
VL	-27.10	-23.10	-24.33	-19.54	-31.30	-31.11
			A-W interface			
Ph	-30.00	-27.30	-27.01			
4-HBA	-21.92	-25.40	-19.38	-18.69	-21.35	-23.34
VL	-31.29	-34.68	-16.62	-22.71	-30.85	-29.35
			TiO_2 clusters			
Ph	-31.22	-21.38	-19.86			
4-HBA	-17.42	-26.57	-17.96	-15.98	-24.45	-16.25
VL	-24.60	-20.40	-20.31	-16.87	-23.57	-31.74

Table S3. Gibbs free energy of activation ($\Delta G^{\ddagger}$) for the HO•-initiated reaction of Ph, 4-HBA, and VL. Unit: kcal mol^{-1}.

Compounds	$R_{RAF}1$	$R_{RAF}2$	$R_{RAF}3$	$R_{RAF}4$	$R_{RAF}5$	$R_{RAF}6$	$R_{HAA}2$	$R_{HAA}3$	$R_{HAA}4$	$R_{HAA}5$	$R_{HAA}6$	$R_{HAA}7$	$R_{HAA}8$	$R_{HAA}9$
						Gas-phase								
Ph	6.37	3.45	7.59	5.57	–	–	6.86	45.19	8.56	–	–	4.08	–	–
4-HBA	10.55	7.42	10.86	10.45	11.80	10.00	10.33	11.70	–	10.30	49.33	7.61	4.87	–
VL	7.85	6.39	7.69	9.32	10.43	10.29	–	33.89	–	10.37	46.96	8.81	4.90	10.47
						Bulk water								
Ph	7.17	5.27	5.60	2.46	–	–	9.03	29.08	6.98	–	–	5.39	–	–
4-HBA	11.22	9.43	9.86	8.01	8.77	6.96	11.22	9.43	–	9.86	8.01	8.77	6.96	–
VL	6.69	6.58	7.72	7.62	6.94	7.69	–	26.74	–	10.63	30.17	10.38	6.38	9.96
						A-W interface								
Ph	6.81	-0.97	7.86	4.38	–	–	6.88	7.03	7.30	–	–	1.95	–	–
4-HBA	12.04	5.35	11.37	9.33	10.82	8.10	11.22	12.74	–	9.38	14.53	8.76	8.17	–
VL	5.24	6.48	3.25	1.67	1.10	3.48	–	10.35	–	8.95	8.89	5.43	1.21	4.60
						TiO_2 clusters								
Ph	4.70	5.14	16.98	11.50	–	–	7.47	12.16	12.48	–	–	4.89	–	–
4-HBA	12.55	8.95	11.47	2.64	12.85	10.20	11.08	8.11	–	11.50	11.45	13.46	4.99	–
VL	-1.88	-3.22	-2.78	-3.81	-0.40	0.40	–	5.78	–	1.73	2.20	-1.05	-7.48	-0.51
$_{VL}^{pre}$	0.00	0.00	0.00	0.00	0.00	0.00	–	17.28	–	0.00	0.00	-0.01	12.30	0.00

$_{VL}^{pre}$**:** $\Delta G^{\ddagger}$ values of free energy difference between transition states and reaction complexes.

Table S4. Gibbs free energy of reaction ($\Delta_r G$) for the HO•-initiated reaction of Ph, 4-HBA, and VL. Unit: kcal mol^{-1}.

Compounds	$R_{RAF}1$	$R_{RAF}2$	$R_{RAF}3$	$R_{RAF}4$	$R_{RAF}5$	$R_{RAF}6$	$R_{HAA}2$	$R_{HAA}3$	$R_{HAA}4$	$R_{HAA}5$	$R_{HAA}6$	$R_{HAA}7$	$R_{HAA}8$	$R_{HAA}9$
Gas-phase														
Ph	-15.85	-15.78	-11.57	-12.81	–	–	-9.92	-10.82	-9.57	–	–	-32.39	–	–
4-HBA	-12.29	-11.73	-9.12	-4.21	-7.88	-8.39	-6.31	-6.51	–	-5.67	-5.17	-27.53	-28.86	–
VL	-16.53	-13.40	-10.20	-6.06	-11.05	-7.33	–	1.66	–	-5.07	-5.26	-29.65	-29.18	-21.19
Bulk water														
Ph	-13.36	-14.77	-16.58	-13.39	–	–	-6.92	-6.43	-6.43	–	–	-31.97		–
4-HBA	-12.38	-9.50	-9.45	-5.31	-11.28	-9.81	-7.96	-8.82	–	-9.33	-8.11	-28.25	-29.34	–
VL	-30.28	-27.25	-24.49	-6.23	-15.18	-8.18	–	-4.75	–	-8.14	-7.70	-34.53	-28.99	-22.24
A-W interface														
Ph	-14.07	-17.70	-11.90	-14.04	–	–	-11.10	-11.77	-10.60	–	–	-31.31	–	–
4-HBA	-11.49	-10.79	-8.10	-9.68	-8.32	-10.06	-6.48	-6.39	–	-7.35	–	-24.50	-29.95	–
VL	-23.74	-7.11	-12.13	-14.08	-14.05	-17.02	–	-4.94	–	-9.06	-6.62	-32.29	-28.21	-22.58
TiO_2 clusters														
Ph	-20.66	-15.51	-10.59	-8.04	–	–	-6.92	-6.43	-6.43	–	–	-31.97	–	–
4-HBA	-17.85	-9.27	-10.91	-2.15	-13.04	-7.96	-5.34	-6.68	–	-8.71	-3.85	-21.60	-20.82	–
VL	-29.72	-21.80	-25.06	-19.88	-25.90	-16.39	–	-29.72	–	-21.80	-25.06	-19.88	-25.90	-16.39

Table S5. The reaction rate constants (k_{uni}/cm^3 molecule^{-1} s^{-1}) for the ozonolysis of Ph, 4-HBA, and VL in different environmental media (EM) over the temperature range of 318 – 278 K.

EM	k	318	308	298	288	278	Γ
				Ph			
A-W	k_1	6.69×10^{-7}	6.33×10^{-7}	5.98×10^{-7}	5.64×10^{-7}	5.32×10^{-7}	100.00%
	k_2	2.50×10^{-17}	1.08×10^{-17}	4.46×10^{-18}	1.73×10^{-18}	6.28×10^{-19}	0.00%
	k_3	2.33×10^{-19}	8.67×10^{-20}	3.03×10^{-20}	9.85×10^{-21}	2.97×10^{-21}	0.00%
	k_{tot}	6.69×10^{-7}	6.33×10^{-7}	5.98×10^{-7}	5.64×10^{-7}	5.32×10^{-7}	100.00%
TiO_2	k_1	2.65×10^{-24}	6.82×10^{-25}	1.61×10^{-25}	3.44×10^{-26}	6.61×10^{-27}	8.73%
	k_2	1.01×10^{-23}	2.71×10^{-24}	6.69×10^{-25}	1.50×10^{-25}	3.04×10^{-26}	36.33%
	k_3	1.48×10^{-23}	4.04×10^{-24}	1.01×10^{-24}	2.31×10^{-25}	4.77×10^{-26}	54.94%
	k_{tot}	2.75×10^{-23}	7.43×10^{-24}	1.84×10^{-24}	4.16×10^{-25}	8.47×10^{-26}	100.00%
Gas phase	k_1	5.76×10^{-20}	5.82×10^{-20}	5.17×10^{-20}	4.88×10^{-20}	4.61×10^{-20}	97.94%
	k_2	4.76×10^{-21}	1.57×10^{-21}	4.79×10^{-22}	1.35×10^{-22}	3.50×10^{-23}	0.91%
	k_3	5.97×10^{-21}	1.98×10^{-21}	6.09×10^{-22}	1.72×10^{-22}	4.42×10^{-23}	1.16%
	k_{tot}	6.83×10^{-20}	6.17×10^{-20}	5.27×10^{-20}	4.91×10^{-20}	4.62×10^{-20}	100.00%
Bulk water	k_1	1.43×10^{12}	1.51×10^{12}	1.59×10^{12}	1.68×10^{12}	1.77×10^{12}	39.58%
	k_2	8.96×10^{11}	9.59×10^{11}	1.03×10^{12}	1.10×10^{12}	1.18×10^{12}	25.56%
	k_3	1.25×10^{12}	1.32×10^{12}	1.40×10^{12}	1.48×10^{12}	1.57×10^{12}	34.86%
	k_{tot}	3.58×10^{12}	3.79×10^{12}	4.02×10^{12}	4.26×10^{12}	4.51×10^{12}	100.00%
				4-HBA			
A-W	k_1	3.74×10^{-22}	1.16×10^{-22}	3.32×10^{-23}	8.76×10^{-24}	2.10×10^{-24}	48.92%
	k_2	2.44×10^{-22}	7.45×10^{-23}	2.10×10^{-23}	5.46×10^{-24}	1.29×10^{-24}	30.98%
	k_3	3.65×10^{-24}	9.73×10^{-25}	2.38×10^{-25}	5.28×10^{-26}	1.05×10^{-26}	0.35%
	k_4	1.54×10^{-24}	3.98×10^{-25}	9.42×10^{-26}	2.03×10^{-26}	3.91×10^{-27}	0.14%
	k_5	1.33×10^{-23}	3.69×10^{-24}	9.44×10^{-25}	2.20×10^{-25}	4.63×10^{-26}	1.39%
	k_6	1.48×10^{-22}	4.45×10^{-23}	1.24×10^{-23}	3.15×10^{-24}	7.31×10^{-25}	18.22%
	k_{tot}	7.85×10^{-22}	2.40×10^{-22}	6.79×10^{-23}	1.77×10^{-23}	4.18×10^{-24}	100.00%

TiO_2	k_1	5.51×10^{-25}	1.38×10^{-25}	3.16×10^{-26}	6.56×10^{-27}	1.22×10^{-27}	0.59%
	k_2	2.33×10^{-23}	6.59×10^{-24}	1.72×10^{-24}	4.08×10^{-25}	8.78×10^{-26}	32.26%
	k_3	1.14×10^{-23}	3.15×10^{-24}	8.00×10^{-25}	1.85×10^{-25}	3.87×10^{-26}	15.02%
	k_4	1.95×10^{-25}	4.73×10^{-26}	1.04×10^{-26}	2.08×10^{-27}	3.70×10^{-28}	0.20%
	k_5	3.64×10^{-23}	1.04×10^{-23}	2.76×10^{-24}	6.68×10^{-25}	1.46×10^{-25}	51.90%
	k_6	2.67×10^{-26}	6.07×10^{-27}	1.25×10^{-27}	2.32×10^{-28}	3.82×10^{-29}	0.02%
	k_{tot}	7.19×10^{-23}	2.04×10^{-23}	5.32×10^{-24}	1.27×10^{-24}	2.74×10^{-25}	100.00%
Gas phase	k_1	2.11×10^{-23}	5.96×10^{-24}	1.55×10^{-24}	3.67×10^{-25}	7.86×10^{-26}	31.36%
	k_2	7.84×10^{-24}	2.14×10^{-24}	5.37×10^{-25}	1.23×10^{-25}	2.53×10^{-26}	10.89%
	k_3	2.88×10^{-24}	7.61×10^{-25}	1.84×10^{-25}	4.06×10^{-26}	8.04×10^{-27}	3.74%
	k_4	6.46×10^{-24}	1.75×10^{-24}	4.37×10^{-25}	9.91×10^{-26}	2.03×10^{-26}	8.85%
	k_5	2.56×10^{-23}	7.27×10^{-24}	1.90×10^{-24}	4.54×10^{-25}	9.80×10^{-26}	38.50%
	k_6	4.95×10^{-24}	1.33×10^{-24}	3.29×10^{-25}	7.39×10^{-26}	1.50×10^{-26}	6.67%
	k_{tot}	6.88×10^{-23}	1.92×10^{-23}	4.93×10^{-24}	1.16×10^{-24}	2.45×10^{-25}	100.00%
Bulk water	k_1	3.10×10^{11}	3.36×10^{11}	3.64×10^{11}	3.95×10^{11}	4.28×10^{11}	18.45%
	k_2	2.61×10^{11}	2.85×10^{11}	3.10×10^{11}	3.37×10^{11}	3.67×10^{11}	15.70%
	k_3	2.15×10^{11}	2.35×10^{11}	2.57×10^{11}	2.81×10^{11}	3.08×10^{11}	13.04%
	k_4	2.74×10^{11}	2.98×10^{11}	3.24×10^{11}	3.52×10^{11}	3.82×10^{11}	16.39%
	k_5	3.28×10^{11}	3.54×10^{11}	3.83×10^{11}	4.14×10^{11}	4.47×10^{11}	19.39%
	k_6	2.84×10^{11}	3.09×10^{11}	3.36×10^{11}	3.65×10^{11}	3.97×10^{11}	17.03%
	k_{tot}	1.67×10^{12}	1.82×10^{12}	1.97×10^{12}	2.14×10^{12}	2.33×10^{12}	100.00%
				VL			
A-W	k_1	6.12×10^{-17}	2.80×10^{-17}	1.21×10^{-17}	4.99×10^{-18}	1.93×10^{-18}	95.90%
	k_2	2.26×10^{-20}	7.97×10^{-21}	2.63×10^{-21}	8.07×10^{-22}	2.28×10^{-22}	0.02%
	k_3	3.18×10^{-18}	1.32×10^{-18}	5.16×10^{-19}	1.90×10^{-19}	6.51×10^{-20}	4.07%
	k_4	6.27×10^{-22}	1.97×10^{-22}	5.74×10^{-23}	1.54×10^{-23}	3.77×10^{-24}	0.00%
	k_5	1.23×10^{-21}	3.96×10^{-22}	1.18×10^{-22}	3.27×10^{-23}	8.23×10^{-24}	0.00%
	k_6	8.00×10^{-21}	2.73×10^{-21}	8.70×10^{-22}	2.57×10^{-22}	6.95×10^{-23}	0.01%
	k_{tot}	6.44×10^{-17}	2.93×10^{-17}	1.27×10^{-17}	5.18×10^{-18}	1.99×10^{-18}	100.00%

TiO_2	k_1	3.63×10^{-18}	1.51×10^{-18}	5.97×10^{-19}	2.21×10^{-19}	7.66×10^{-20}	0.02%
	k_2	4.83×10^{-15}	2.54×10^{-15}	1.29×10^{-15}	6.22×10^{-16}	2.86×10^{-16}	38.91%
	k_3	3.51×10^{-19}	1.36×10^{-19}	4.93×10^{-20}	1.68×10^{-20}	5.28×10^{-21}	0.00%
	k_4	7.19×10^{-15}	3.83×10^{-15}	1.96×10^{-15}	9.63×10^{-16}	4.50×10^{-16}	59.44%
	k_5	2.22×10^{-16}	1.06×10^{-16}	4.82×10^{-17}	2.08×10^{-17}	8.48×10^{-18}	1.46%
	k_6	3.01×10^{-17}	1.35×10^{-17}	5.71×10^{-18}	2.29×10^{-18}	8.63×10^{-19}	0.17%
	k_{tot}	1.23×10^{-14}	6.50×10^{-15}	3.30×10^{-15}	1.61×10^{-15}	7.46×10^{-16}	100.00%
Gas-phase	k_1	1.05×10^{-22}	3.10×10^{-23}	8.51×10^{-24}	2.14×10^{-24}	4.87×10^{-25}	6.32%
	k_2	5.11×10^{-24}	1.38×10^{-24}	3.40×10^{-25}	7.63×10^{-26}	1.54×10^{-26}	0.25%
	k_3	1.19×10^{-21}	3.81×10^{-22}	1.13×10^{-22}	3.11×10^{-23}	7.82×10^{-24}	84.30%
	k_4	4.76×10^{-25}	1.19×10^{-25}	2.70×10^{-26}	5.54×10^{-27}	1.02×10^{-27}	0.02%
	k_5	1.16×10^{-22}	3.46×10^{-23}	9.54×10^{-24}	2.41×10^{-24}	5.52×10^{-25}	7.09%
	k_6	3.58×10^{-23}	1.03×10^{-23}	2.71×10^{-24}	6.55×10^{-25}	1.43×10^{-25}	2.02%
	k_{tot}	1.45×10^{-21}	4.58×10^{-22}	1.35×10^{-22}	3.64×10^{-23}	9.02×10^{-24}	100.00%
Bulk water	k_1	3.455×10^{11}	3.712×10^{11}	3.986×10^{11}	4.278×10^{11}	4.590×10^{11}	18.08%
	k_2	2.671×10^{11}	2.897×10^{11}	3.142×10^{11}	3.406×10^{11}	3.691×10^{11}	14.25%
	k_3	4.161×10^{11}	4.437×10^{11}	4.728×10^{11}	5.036×10^{11}	5.362×10^{11}	21.45%
	k_4	1.479×10^{11}	1.631×10^{11}	1.798×10^{11}	1.980×10^{11}	2.181×10^{11}	8.16%
	k_5	4.005×10^{11}	4.302×10^{11}	4.619×10^{11}	4.960×10^{11}	5.326×10^{11}	20.96%
	k_6	3.253×10^{11}	3.501×10^{11}	3.767×10^{11}	4.052×10^{11}	4.357×10^{11}	17.09%
	k_{tot}	1.90×10^{12}	2.05×10^{12}	2.20×10^{12}	2.37×10^{12}	2.55×10^{12}	100.00%

Table S6. The reaction rate constants (k_{uni}/cm^3 molecule $^{-1}$ s $^{-1}$) for the HO$^{\bullet}$-initiated reaction of Ph, 4-HBA, and VL in different environmental media (EM) over the temperature range of 318 – 278 K.

EM	k	318	308	298	288	278	Γ
				Ph-R_{RAF}			
	k_1	7.33×10^{-12}	4.90×10^{-12}	3.20×10^{-12}	2.03×10^{-12}	1.25×10^{-12}	0.00%
	k_2	2.74×10^{-6}	2.70×10^{-6}	2.67×10^{-6}	2.64×10^{-6}	2.62×10^{-6}	99.15%
	k_3	2.77×10^{-12}	1.75×10^{-12}	1.08×10^{-12}	6.44×10^{-13}	3.71×10^{-13}	0.00%
	k_4	3.27×10^{-10}	2.47×10^{-10}	1.84×10^{-10}	1.34×10^{-10}	9.59×10^{-11}	0.01%
	k_{totRAF}	2.74×10^{-6}	2.70×10^{-6}	2.67×10^{-6}	2.64×10^{-6}	2.62×10^{-6}	99.16%
A-W				Ph-R_{HAA}ben			
	k_1	2.09×10^{-11}	1.42×10^{-11}	9.43×10^{-12}	6.10×10^{-12}	3.83×10^{-12}	0.00%
	k_2	1.87×10^{-11}	1.27×10^{-11}	8.39×10^{-12}	5.40×10^{-12}	3.37×10^{-12}	0.00%
	k_3	6.47×10^{-12}	4.33×10^{-12}	2.82×10^{-12}	1.79×10^{-12}	1.10×10^{-12}	0.00%
	$k_{totHAAben}$	4.61×10^{-11}	3.12×10^{-11}	2.06×10^{-11}	1.33×10^{-11}	8.30×10^{-12}	0.00%
				Ph-R_{HAA}sub			
	k_7	2.95×10-8	2.59×10^{-8}	2.26×10^{-8}	1.96×10^{-8}	1.69×10^{-8}	0.84%
	$k_{totHAAsub}$	2.95×10^{-8}	2.59×10^{-8}	2.26×10^{-8}	1.96×10^{-8}	1.69×10^{-8}	0.84%
	k_{tot}	2.77×10^{-6}	2.73×10^{-6}	2.69×10^{-6}	2.66×10^{-6}	2.63×10^{-6}	100.00%
				Ph-R_{RAF}			
	k_1	1.71×10^{-10}	1.51×10^{-10}	1.11×10^{-10}	7.93×10^{-11}	5.57×10^{-11}	34.90%
	k_2	1.91×10^{-10}	1.38×10^{-10}	9.85×10^{-11}	6.86×10^{-11}	4.67×10^{-11}	31.10%
	k_3	1.58×10^{-18}	6.28×10^{-19}	2.35×10^{-19}	8.26×10^{-20}	2.70×10^{-20}	0.00%
	k_4	4.55×10^{-15}	2.39×10^{-15}	1.21×10^{-15}	5.85×10^{-16}	2.69×10^{-16}	0.00%
	k_{totRAF}	3.62×10^{-10}	2.89×10^{-10}	2.10×10^{-10}	1.48×10^{-10}	1.02×10^{-10}	66.00%
TiO_2				Ph-R_{HAA}ben			
	k_1	1.09×10^{-11}	7.26×10^{-12}	4.71×10^{-12}	2.97×10^{-12}	1.81×10^{-12}	1.49%
	k_2	7.09×10^{-15}	3.71×10^{-15}	1.86×10^{-15}	8.94×10^{-16}	4.07×10^{-16}	0.00%
	k_3	2.12×10^{-15}	1.09×10^{-15}	5.39×10^{-16}	2.54×10^{-16}	1.13×10^{-16}	0.00%

	$k_{totHAAben}$	1.09×10^{-11}	7.26×10^{-12}	4.71×10^{-12}	2.97×10^{-12}	1.81×10^{-12}	1.49%
				Ph-R_{HAA}sub			
	k_7	1.88×10^{-10}	1.41×10^{-10}	1.03×10^{-10}	7.40×10^{-11}	5.21×10^{-11}	32.51%
	$k_{totHAAsub}$	1.88×10^{-10}	1.41×10^{-10}	1.03×10^{-10}	7.40×10^{-11}	5.21×10^{-11}	32.51%
	k_{tot}	5.61×10^{-10}	4.37×10^{-10}	3.17×10^{-10}	2.25×10^{-10}	1.56×10^{-10}	100.00%
				Ph-R_{RAF}			
	k_1	1.41×10^{-11}	9.64×10^{-12}	6.43×10^{-12}	4.18×10^{-12}	2.64×10^{-12}	0.27%
	k_2	2.69×10^{-9}	2.13×10^{-9}	1.66×10^{-9}	1.27×10^{-9}	9.62×10^{-10}	70.73%
	k_3	4.38×10^{-12}	2.82×10^{-12}	1.76×10^{-12}	1.07×10^{-12}	6.29×10^{-13}	0.08%
	k_4	5.01×10^{-11}	3.56×10^{-11}	2.48×10^{-11}	1.69×10^{-11}	1.12×10^{-11}	1.06%
	k_{totRAF}	2.76×10^{-9}	2.18×10^{-9}	1.69×10^{-9}	1.29×10^{-9}	9.76×10^{-10}	72.14%
Gas phase				Ph-R_{HAA}ben			
	k_1	2.56×10^{-11}	1.75×10^{-11}	1.17×10^{-11}	7.60×10^{-12}	4.81×10^{-12}	0.50%
	k_2	1.02×10^{-36}	9.93×10^{-38}	8.31×10^{-39}	5.85×10^{-40}	3.41×10^{-41}	0.00%
	k_3	9.16×10^{-13}	5.75×10^{-13}	3.50×10^{-13}	2.07×10^{-13}	1.18×10^{-13}	0.01%
	k_{totHAn}	2.65×10^{-11}	1.81×10^{-11}	1.21×10^{-11}	7.81×10^{-12}	4.93×10^{-12}	0.51%
				Ph-R_{HAA}sub			
	k_7	1.04×10^{-9}	8.24×10^{-10}	6.41×10^{-10}	4.91×10^{-10}	3.70×10^{-10}	27.34%
	$k_{totHAAsub}$	1.04×10^{-9}	8.24×10^{-10}	6.41×10^{-10}	4.91×10^{-10}	3.70×10^{-10}	27.34%
	k_{tot}	3.83×10^{-9}	3.02×10^{-9}	2.34×10^{-9}	1.79×10^{-9}	1.35×10^{-9}	100.00%
				Ph-R_{RAF}			
	k_1	2.45×10^{12}	2.49×10^{12}	2.52×10^{12}	2.55×10^{12}	2.59×10^{12}	5.65%
	k_2	6.19×10^{12}	6.19×10^{12}	6.19×10^{12}	6.18×10^{12}	6.17×10^{12}	13.86%
	k_3	6.71×10^{12}	6.77×10^{12}	6.83×10^{12}	6.90×10^{12}	6.96×10^{12}	15.32%
	k_4	5.20×10^{12}	5.15×10^{12}	5.09×10^{12}	5.04×10^{12}	4.98×10^{12}	11.41%
	k_{totRAF}	2.06×10^{13}	2.06×10^{13}	2.06×10^{13}	2.07×10^{13}	2.07×10^{13}	46.24%
Bulk water				Ph-R_{HAA}ben			
	k_1	7.14×10^{12}	7.50×10^{12}	7.90×10^{12}	8.32×10^{12}	8.78×10^{12}	17.70%
	k_2	2.51×10^{12}	3.00×10^{12}	3.57×10^{12}	4.27×10^{12}	5.10×10^{12}	8.01%

	k_3	5.21×10^{12}	5.43×10^{12}	5.66×10^{12}	5.91×10^{12}	6.19×10^{12}	12.69%
	$k_{totHAAben}$	1.49×10^{13}	1.59×10^{13}	1.71×10^{13}	1.85×10^{13}	2.01×10^{13}	38.40%
				Ph-R_{HAA}sub			
	k_7	6.42×10^{12}	6.63×10^{12}	6.85×10^{12}	7.09×10^{12}	7.35×10^{12}	15.36%
	$k_{totHAAsub}$	6.42×10^{12}	6.63×10^{12}	6.85×10^{12}	7.09×10^{12}	7.35×10^{12}	15.36%
	k_{tot}	4.18×10^{13}	4.32×10^{13}	4.46×10^{13}	4.63×10^{13}	4.81×10^{13}	100.00%
				4-HBA-R_{RAF}			
	k_1	1.95×10^{-15}	9.98×10^{-16}	4.90×10^{-16}	2.30×10^{-16}	1.02×10^{-16}	0.00%
	k_2	6.50×10^{-11}	4.65×10^{-11}	3.26×10^{-11}	2.23×10^{-11}	1.49×10^{-11}	34.34%
	k_3	5.74×10^{-15}	3.05×10^{-15}	1.55×10^{-15}	7.58×10^{-16}	3.52×10^{-16}	0.00%
	k_4	1.29×10^{-13}	7.55×10^{-14}	4.28×10^{-14}	2.33×10^{-14}	1.22×10^{-14}	0.05%
	k_5	1.34×10^{-14}	7.30×10^{-15}	3.83×10^{-15}	1.93×10^{-15}	9.26×10^{-16}	0.00%
	k_6	9.21×10^{-13}	5.75×10^{-13}	3.49×10^{-13}	2.05×10^{-13}	1.16×10^{-13}	0.37%
	k_{totRAF}	6.61×10^{-11}	4.72×10^{-11}	3.30×10^{-11}	2.25×10^{-11}	1.50×10^{-11}	34.76%
A-W				4-HBA-R_{HAA}ben			
	k_2	1.48×10^{-14}	8.12×10^{-15}	4.29×10^{-15}	2.18×10^{-15}	1.05×10^{-15}	0.00%
	k_3	1.99×10^{-12}	1.28×10^{-12}	7.99×10^{-13}	4.85×10^{-13}	2.84×10^{-13}	0.84%
	k_5	8.95×10^{-15}	4.83×10^{-15}	2.51×10^{-15}	1.25×10^{-15}	5.90×10^{-16}	0.00%
	k_6	1.11×10^{-14}	6.02×10^{-15}	3.15×10^{-15}	1.57×10^{-15}	7.50×10^{-16}	0.00%
	$k_{totHAAben}$	2.02×10^{-12}	1.30×10^{-12}	8.09×10^{-13}	4.90×10^{-13}	2.86×10^{-13}	0.84%
				4-HBA-R_{HAA}sub			
	k_7	5.57×10^{-16}	2.74×10^{-16}	1.29×10^{-16}	5.74×10^{-17}	2.42×10^{-17}	0.00%
	k_8	1.17×10^{-10}	8.53×10^{-11}	6.11×10^{-11}	4.28×10^{-11}	2.94×10^{-11}	64.39%
	$k_{totHAAsub}$	1.17×10^{-10}	8.53×10^{-11}	6.11×10^{-11}	4.28×10^{-11}	2.94×10^{-11}	64.39%
	k_{tot}	1.85×10^{-10}	1.34×10^{-10}	9.49×10^{-11}	6.59×10^{-11}	4.47×10^{-11}	100.00%
				4-HBA-R_{RAF}			
	k_1	8.61×10^{-16}	4.29×10^{-16}	2.05×10^{-16}	9.31×10^{-17}	4.01×10^{-17}	0.00%
TiO_2	k_2	2.38×10^{-13}	1.42×10^{-13}	8.21×10^{-14}	4.59×10^{-14}	2.46×10^{-14}	0.00%
	k_3	5.00×10^{-15}	2.64×10^{-15}	1.34×10^{-15}	6.51×10^{-16}	3.01×10^{-16}	0.00%

	k_4	4.72×10^{-9}	3.88×10^{-9}	3.16×10^{-9}	2.54×10^{-9}	2.01×10^{-9}	99.96%
	k_5	5.36×10^{-16}	2.63×10^{-16}	1.24×10^{-16}	5.52×10^{-17}	2.33×10^{-17}	0.00%
	k_6	3.71×10^{-14}	2.09×10^{-14}	1.14×10^{-14}	5.96×10^{-15}	2.98×10^{-15}	0.00%
	k_{totRAF}	4.72×10^{-9}	3.88×10^{-9}	3.16×10^{-9}	2.54×10^{-9}	2.01×10^{-9}	99.96%
				4-HBA-R_{HAA}ben			
	k_2	1.62×10^{-14}	8.90×10^{-15}	4.71×10^{-15}	2.39×10^{-15}	1.15×10^{-15}	0.00%
	k_3	1.52×10^{-15}	7.76×10^{-16}	3.78×10^{-16}	1.76×10^{-16}	7.72×10^{-17}	0.00%
	k_5	1.98×10^{-13}	1.19×10^{-13}	6.86×10^{-14}	3.83×10^{-14}	2.05×10^{-14}	0.00%
	k_6	9.78×10^{-17}	4.55×10^{-17}	2.01×10^{-17}	8.42×10^{-18}	3.32×10^{-18}	0.00%
	$k_{totHAAben}$	2.16×10^{-13}	1.29×10^{-13}	7.37×10^{-14}	4.09×10^{-14}	2.17×10^{-14}	0.00%
				4-HBA-R_{HAA}sub			
	k_7	1.34×10^{-12}	8.44×10^{-13}	5.16×10^{-13}	3.05×10^{-13}	1.74×10^{-13}	0.02%
	k_8	1.22×10^{-12}	7.71×10^{-13}	4.75×10^{-13}	2.83×10^{-13}	1.63×10^{-13}	0.02%
	$k_{totHAAsub}$	2.56×10^{-12}	1.62×10^{-12}	9.91×10^{-13}	5.88×10^{-13}	3.37×10^{-13}	0.04%
	k_{tot}	4.72×10^{-9}	3.88×10^{-9}	3.16×10^{-9}	2.54×10^{-9}	2.01×10^{-9}	100.00%
				4-HBA-R_{RAF}			
	k_1	1.99×10^{-14}	1.10×10^{-14}	5.84×10^{-15}	2.98×10^{-15}	1.45×10^{-15}	0.01%
	k_2	2.57×10^{-12}	1.66×10^{-12}	1.04×10^{-12}	6.34×10^{-13}	3.74×10^{-13}	1.32%
	k_3	1.25×10^{-14}	6.81×10^{-15}	3.57×10^{-15}	1.79×10^{-15}	8.57×10^{-16}	0.00%
	k_4	2.21×10^{-14}	1.22×10^{-14}	6.53×10^{-15}	3.34×10^{-15}	1.63×10^{-15}	0.01%
	k_5	2.90×10^{-15}	1.50×10^{-15}	7.49×10^{-16}	3.56×10^{-16}	1.61×10^{-16}	0.00%
Gas-phase	k_6	4.64×10^{-14}	2.63×10^{-14}	1.44×10^{-14}	7.59×10^{-15}	3.82×10^{-15}	0.02%
	k_{totRAF}	2.67×10^{-12}	1.72×10^{-12}	1.07×10^{-12}	6.50×10^{-13}	3.82×10^{-13}	1.36%
				4-HBA-R_{HAA}ben			
	k_2	5.70×10^{-14}	3.27×10^{-14}	1.81×10^{-14}	9.63×10^{-15}	4.91×10^{-15}	0.02%
	k_3	6.73×10^{-15}	3.60×10^{-15}	1.85×10^{-15}	9.09×10^{-16}	4.25×10^{-16}	0.00%
	k_5	7.77×10^{-14}	4.49×10^{-14}	2.50×10^{-14}	1.34×10^{-14}	6.90×10^{-15}	0.03%
	k_6	4.93×10^{-40}	3.89×10^{-41}	2.59×10^{-42}	1.43×10^{-43}	6.41×10^{-45}	0.00%
	$k_{totHAAben}$	1.41×10^{-13}	8.12×10^{-14}	4.50×10^{-14}	2.39×10^{-14}	1.22×10^{-14}	0.05%

				4-HBA-R_{HAA}sub			
	k_7	5.84×10^{-12}	3.88×10^{-12}	2.51×10^{-12}	1.58×10^{-12}	9.61×10^{-13}	3.18%
	k_8	1.42×10^{-10}	1.04×10^{-10}	7.53×10^{-11}	5.32×10^{-11}	3.68×10^{-11}	95.41%
	$k_{totHAAsub}$	1.48×10^{-10}	1.08×10^{-10}	7.78×10^{-11}	5.48×10^{-11}	3.78×10^{-11}	98.59%
	k_{tot}	1.51×10^{-10}	1.10×10^{-10}	7.90×10^{-11}	5.55×10^{-11}	3.81×10^{-11}	100.00%
				4-HBA-R_{RAF}			
	k_1	1.34×10^{12}	1.39×10^{12}	1.44×10^{12}	1.49×10^{12}	1.55×10^{12}	5.71%
	k_2	1.62×10^{12}	1.66×10^{12}	1.69×10^{12}	1.73×10^{12}	1.76×10^{12}	6.71%
	k_3	1.72×10^{12}	1.77×10^{12}	1.83×10^{12}	1.88×10^{12}	1.94×10^{12}	7.25%
	k_4	2.13×10^{12}	2.17×10^{12}	2.20×10^{12}	2.24×10^{12}	2.28×10^{12}	8.75%
	k_5	2.09×10^{12}	2.14×10^{12}	2.20×10^{12}	2.26×10^{12}	2.32×10^{12}	8.73%
	k_6	2.60×10^{12}	2.64×10^{12}	2.68×10^{12}	2.71×10^{12}	2.75×10^{12}	10.62%
	k_{totRAF}	1.15×10^{13}	1.18×10^{13}	1.20×10^{13}	1.23×10^{13}	1.26×10^{13}	47.77%
Bulk water				4-HBA-R_{HAA}ben			
	k_2	2.14×10^{12}	2.30×10^{12}	2.47×10^{12}	2.65×10^{12}	2.86×10^{12}	9.80%
	k_3	4.13×10^{10}	5.02×10^{10}	6.12×10^{10}	7.48×10^{10}	9.14×10^{10}	0.24%
	k_5	4.24×10^{12}	4.52×10^{12}	4.82×10^{12}	5.15×10^{12}	5.50×10^{12}	19.13%
	k_6	3.54×10^{11}	4.33×10^{11}	5.30×10^{11}	6.50×10^{11}	7.98×10^{11}	2.10%
	$k_{totHAAben}$	6.78×10^{12}	7.30×10^{12}	7.88×10^{12}	8.52×10^{12}	9.25×10^{12}	31.27%
				4-HBA-R_{HAA}sub			
	k_7	1.90×10^{12}	2.08×10^{12}	2.28×10^{12}	2.51×10^{12}	2.76×10^{12}	9.06%
	k_8	2.99×10^{12}	3.00×10^{12}	3.00×10^{12}	3.00×10^{12}	3.00×10^{12}	11.90%
	$k_{totHAAsub}$	4.89×10^{12}	5.08×10^{12}	5.28×10^{12}	5.51×10^{12}	5.76×10^{12}	20.96%
	k_{tot}	2.32×10^{13}	2.41×10^{13}	2.52×10^{13}	2.63×10^{13}	2.76×10^{13}	100.00%
				VL-R_{RAF}			
	k_1	7.87×10^{-11}	5.67×10^{-11}	4.00×10^{-11}	2.77×10^{-11}	1.87×10^{-11}	0.02%
A-W	k_2	1.15×10^{-11}	7.78×10^{-12}	5.15×10^{-12}	3.32×10^{-12}	2.08×10^{-12}	0.00%
	k_3	1.96×10^{-9}	1.57×10^{-9}	1.24×10^{-9}	9.69×10^{-10}	7.44×10^{-10}	0.72%
	k_4	2.10×10^{-8}	1.81×10^{-8}	1.55×10^{-8}	1.31×10^{-8}	1.10×10^{-8}	8.98%

	k_5	5.13×10^{-8}	4.55×10^{-8}	4.02×10^{-8}	3.52×10^{-8}	3.06×10^{-8}	23.27%
	k_6	1.28×10^{-9}	1.01×10^{-9}	7.88×10^{-10}	6.04×10^{-10}	4.55×10^{-10}	0.46%
	k_{totRAF}	7.57×10^{-8}	6.63×10^{-8}	5.77×10^{-8}	4.99×10^{-8}	4.29×10^{-8}	33.46%
				VL-R_{HAA}ben			
	k_3	7.17×10^{-14}	4.13×10^{-14}	2.30×10^{-14}	1.23×10^{-14}	6.30×10^{-15}	0.00%
	k_5	5.47×10^{-13}	3.37×10^{-13}	2.02×10^{-13}	1.17×10^{-13}	6.49×10^{-14}	0.00%
	k_6	2.33×10^{-13}	1.38×10^{-13}	7.98×10^{-14}	4.43×10^{-14}	2.37×10^{-14}	0.00%
	$k_{totHAAben}$	8.51×10^{-13}	5.17×10^{-13}	3.04×10^{-13}	1.73×10^{-13}	9.49×10^{-14}	0.00%
				VL-R_{HAA}sub			
	k_7	2.99×10^{-10}	2.23×10^{-10}	1.64×10^{-10}	1.18×10^{-10}	8.31×10^{-11}	0.10%
	k_8	1.35×10^{-7}	1.25×10^{-7}	1.14×10^{-7}	1.05×10^{-7}	9.51×10^{-8}	66.36%
	k_9	2.78×10^{-10}	2.10×10^{-10}	1.56×10^{-10}	1.14×10^{-10}	8.11×10^{-11}	0.09%
	$k_{totHAAsub}$	1.36×10^{-7}	1.25×10^{-7}	1.15×10^{-7}	1.05×10^{-7}	9.53×10^{-8}	66.54%
	k_{tot}	2.12×10^{-7}	1.91×10^{-7}	1.73×10^{-7}	1.55×10^{-7}	1.38×10^{-7}	100.00%
				VL-R_{RAF}			
	k_1	3.78×10^{-7}	3.59×10^{-7}	3.42×10^{-7}	3.25×10^{-7}	3.09×10^{-7}	5.11%
	k_2	3.39×10^{-7}	3.21×10^{-7}	3.04×10^{-7}	2.87×10^{-7}	2.71×10^{-7}	4.53%
	k_3	3.47×10^{-7}	3.29×10^{-7}	3.12×10^{-7}	2.95×10^{-7}	2.78×10^{-7}	4.65%
	k_4	3.18×10^{-7}	3.00×10^{-7}	2.82×10^{-7}	2.66×10^{-7}	2.49×10^{-7}	4.22%
TiO_2	k_5	3.77×10^{-7}	3.59×10^{-7}	3.42×10^{-7}	3.25×10^{-7}	3.09×10^{-7}	5.11%
	k_6	3.58×10^{-7}	3.40×10^{-7}	3.23×10^{-7}	3.06×10^{-7}	2.90×10^{-7}	4.82%
	k_{totRAF}	2.12×10^{-6}	2.01×10^{-6}	1.91×10^{-6}	1.80×10^{-6}	1.71×10^{-6}	28.44%
				VL-R_{HAA}ben			
	k_3	1.28×10^{-18}	5.16×10^{-19}	1.96×10^{-19}	7.00×10^{-20}	2.32×10^{-20}	0.00%
	k_5	9.66×10^{-7}	9.47×10^{-7}	9.30×10^{-7}	9.13×10^{-7}	8.97×10^{-7}	13.88%
	k_6	9.35×10^{-7}	9.17×10^{-7}	9.00×10^{-7}	8.83×10^{-7}	8.67×10^{-7}	13.44%
	$k_{totHAAben}$	1.90×10^{-6}	1.86×10^{-6}	1.83×10^{-6}	1.80×10^{-6}	1.76×10^{-6}	27.32%
				VL-R_{HAA}sub			
	k_7	2.55×10^{-6}	2.53×10^{-6}	2.52×10^{-6}	2.50×10^{-6}	2.49×10^{-6}	37.59%

	k_8	4.00×10^{-15}	2.09×10^{-15}	1.05×10^{-15}	5.02×10^{-16}	2.28×10^{-16}	0.00%
	k_9	4.81×10^{-7}	4.63×10^{-7}	4.46×10^{-7}	4.29×10^{-7}	4.13×10^{-7}	6.65%
	$k_{totHAAsub}$	3.03×10^{-6}	2.99×10^{-6}	2.97×10^{-6}	2.93×10^{-6}	2.90×10^{-6}	44.24%
	k_{tot}	7.05×10^{-6}	6.87×10^{-6}	6.70×10^{-6}	6.53×10^{-6}	6.37×10^{-6}	100.00%
				VL-R_{RAF}			
	k_1	1.27×10^{-12}	7.97×10^{-13}	4.88×10^{-13}	2.89×10^{-13}	1.66×10^{-13}	0.43%
	k_2	1.34×10^{-11}	9.12×10^{-12}	6.06×10^{-12}	3.93×10^{-12}	2.47×10^{-12}	5.30%
	k_3	1.75×10^{-12}	1.11×10^{-12}	6.91×10^{-13}	4.16×10^{-13}	2.42×10^{-13}	0.60%
	k_4	1.16×10^{-13}	6.77×10^{-14}	3.81×10^{-14}	2.06×10^{-14}	1.07×10^{-14}	0.03%
	k_5	2.00×10^{-14}	1.10×10^{-14}	5.82×10^{-15}	2.95×10^{-15}	1.43×10^{-15}	0.01%
	k_6	2.71×10^{-14}	1.51×10^{-14}	8.08×10^{-15}	4.16×10^{-15}	2.04×10^{-15}	0.01%
	k_{totRAF}	1.66×10^{-11}	1.11×10^{-11}	7.29×10^{-12}	4.66×10^{-12}	2.89×10^{-12}	6.38%
				VL-R_{HAA}ben			
Gas phase	k_3	1.76×10^{-29}	3.07×10^{-30}	4.77×10^{-31}	6.50×10^{-32}	7.69×10^{-33}	0.00%
	k_5	6.93×10^{-14}	3.99×10^{-14}	2.22×10^{-14}	1.18×10^{-14}	6.05×10^{-15}	0.02%
	k_6	2.37×10^{-38}	2.11×10^{-39}	1.60×10^{-40}	1.02×10^{-41}	5.30×10^{-43}	0.00%
	$k_{totHAAben}$	6.93×10^{-14}	3.99×10^{-14}	2.22×10^{-14}	1.18×10^{-14}	6.05×10^{-15}	0.02%
				VL-R_{HAA}sub			
	k_7	9.26×10^{-13}	5.79×10^{-13}	3.51×10^{-13}	2.06×10^{-13}	1.17×10^{-13}	0.31%
	k_8	1.95×10^{-10}	1.46×10^{-10}	1.07×10^{-10}	7.69×10^{-11}	5.42×10^{-11}	93.30%
	k_9	1.98×10^{-14}	1.09×10^{-14}	5.78×10^{-15}	2.94×10^{-15}	1.43×10^{-15}	0.01%
	$k_{totHAAsub}$	1.96×10^{-10}	1.47×10^{-10}	1.07×10^{-10}	7.71×10^{-11}	5.43×10^{-11}	93.62%
	k_{tot}	2.12×10^{-10}	1.57×10^{-10}	1.14×10^{-10}	8.18×10^{-11}	5.73×10^{-11}	100.00%
				VL-R_{RAF}			
	k_1	2.45×10^{12}	2.47×10^{12}	2.49×10^{12}	2.50×10^{12}	2.51×10^{12}	7.90%
Bulk water	k_2	2.60×10^{12}	2.63×10^{12}	2.65×10^{12}	2.67×10^{12}	2.69×10^{12}	8.41%
	k_3	2.24×10^{12}	2.28×10^{12}	2.31×10^{12}	2.35×10^{12}	2.38×10^{12}	7.34%
	k_4	1.98×10^{12}	1.99×10^{12}	2.01×10^{12}	2.02×10^{12}	2.02×10^{12}	6.37%

k_5	2.20×10^{12}	2.21×10^{12}	2.22×10^{12}	2.22×10^{12}	2.22×10^{12}	7.05%
k_6	2.11×10^{12}	2.14×10^{12}	2.16×10^{12}	2.19×10^{12}	2.21×10^{12}	6.88%
k_{totRAF}	1.36×10^{13}	1.37×10^{13}	1.38×10^{13}	1.40×10^{13}	1.40×10^{13}	43.95%
			VL-R_{HAA}ben			
k_3	1.08×10^{12}	1.27×10^{12}	1.49×10^{12}	1.75×10^{12}	2.07×10^{12}	4.73%
k_5	3.83×10^{12}	4.09×10^{12}	4.38×10^{12}	4.69×10^{12}	5.02×10^{12}	13.90%
k_6	8.04×10^{11}	9.63×10^{11}	1.15×10^{12}	1.38×10^{12}	1.66×10^{12}	3.66%
$k_{totHAAben}$	5.71×10^{12}	6.32×10^{12}	7.02×10^{12}	7.82×10^{12}	8.75×10^{12}	22.29%
			VL-R_{HAA}sub			
k_7	4.52×10^{12}	4.84×10^{12}	5.18×10^{12}	5.55×10^{12}	5.96×10^{12}	16.45%
k_8	3.75×10^{12}	3.84×10^{12}	3.93×10^{12}	4.03×10^{12}	4.14×10^{12}	12.49%
k_9	1.45×10^{12}	1.48×10^{12}	1.51×10^{12}	1.55×10^{12}	1.58×10^{12}	4.81%
$k_{totHAAsub}$	9.72×10^{12}	1.02×10^{13}	1.06×10^{13}	1.11×10^{13}	1.17×10^{13}	33.75%
k_{tot}	2.90×10^{13}	3.02×10^{13}	3.15×10^{13}	3.29×10^{13}	3.45×10^{13}	100.00%

Table S7. Criteria set of the acute (LC_{50}/EC_{50}) and chronic toxicity (ChV) . (mg L^{-1})

Classification	Acute toxicity[1]	Chronic toxicity[2]
Not harmful	LC_{50}>100 or EC_{50}>100	ChV>10
Harmful	10< LC_{50} <100 or 10< EC_{50} <100	1< ChV <10
Toxic	1< LC_{50} <10 or 1< EC_{50} <10	0.1< ChV <1
Very toxic	LC_{50} <1 or EC_{50} <1	ChV<0.1

[1] Criteria set by the European Union (described in Annex VI of Directive 67/548/EEC); [2]Criteria set by the Chinese hazard evaluation guidelines for new chemical substances (HJ/T 154–2004).

Table S8. Acute and chronic toxicity of Ph, 4-HBA, VL and their products. (mg L^{-1})

Compounds	LC50 fish	LC50 daphnid	LC50 Green Algae	ChV fish	ChV daphnid	ChV Green Algae
Ph	27.70	9.64	2.40	2.61	0.97	4.53
4-HBA	17.30	17.00	9.19	3.61	0.17	3.20
VL	19.80	19.20	10.50	3.95	0.19	3.70
P1	7.29	10.20	1.84	0.65	1.72	0.59
P2	22.20	256.00	4.90	14.20	101.00	0.57
P3	27.60	325.00	5.87	17.80	129.00	0.68
P4	129.00	2.23E+3	15.60	96.20	940.00	1.55
P5	491.00	162.00	42.30	45.70	25.90	77.70
P6	336.00	4420.00	75.20	238.00	1760.00	8.57
P7	315.00	1530.00	72.00	199.00	1400.00	8.43
P8	3220.00	67500.00	291.00	2590.00	2930.00	27.00
P9	579.00	2460.00	136.00	5430.00	869.00	1300.00
P10	19.20	73.00	3.45	81.30	16.70	30.70
P11	121.00	143.00	62.40	66.20	0.96	16.00

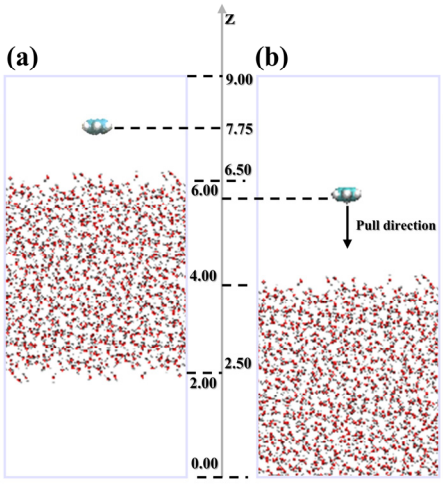

Fig. S1 Schematic representation the initial configuration of **(a)** the umbrella sampling simulation and **(b)** the 150 ns NVT simulation (unit: nm).

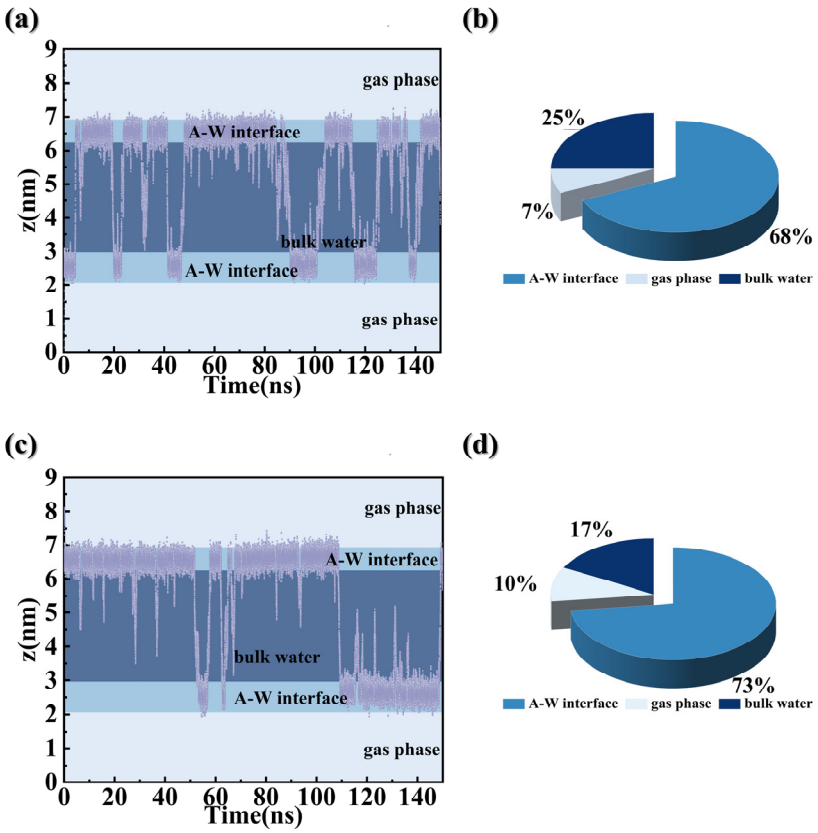

Fig S2 The z coordinates of **(a)** 4-HBA and **(c)** as the function of 150 ns simulation time; the pie chart with the probability of **(b)** O_3 and **(d)** Ph at the A-W interface, in air, and in bulk water.

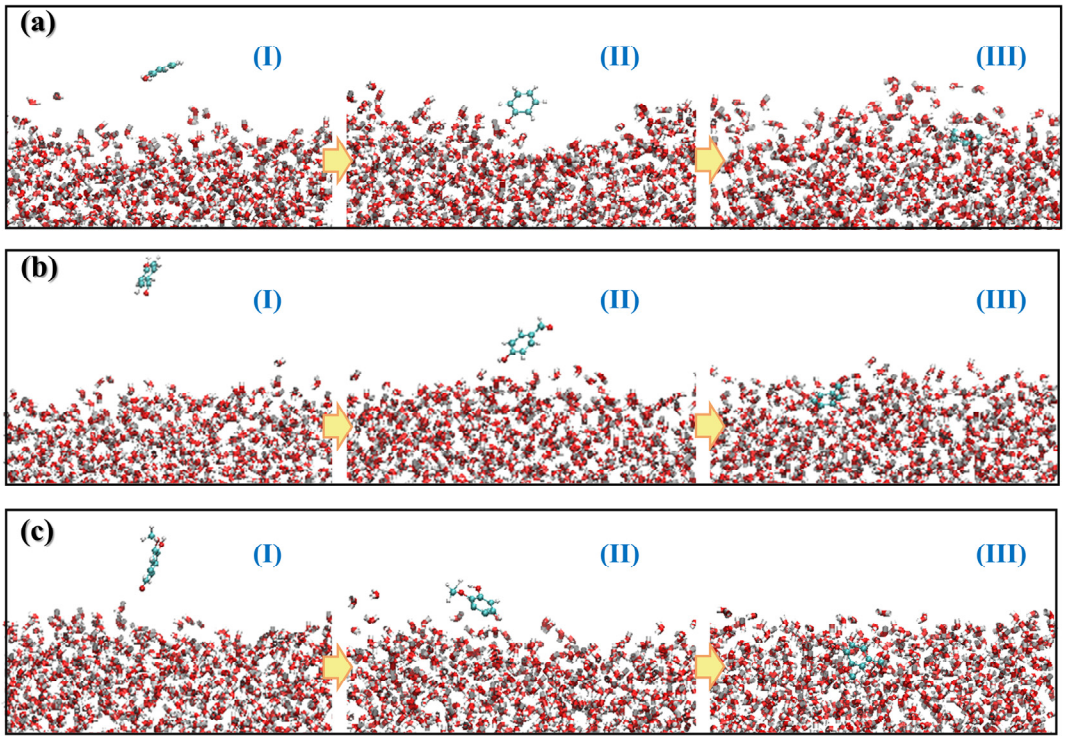

Fig. S3 Typical snapshots from the trajectories of **(a)** Ph, **(b)** 4-HBA, and **(c)** VL diffuse through the interior of the water slab from the air region.

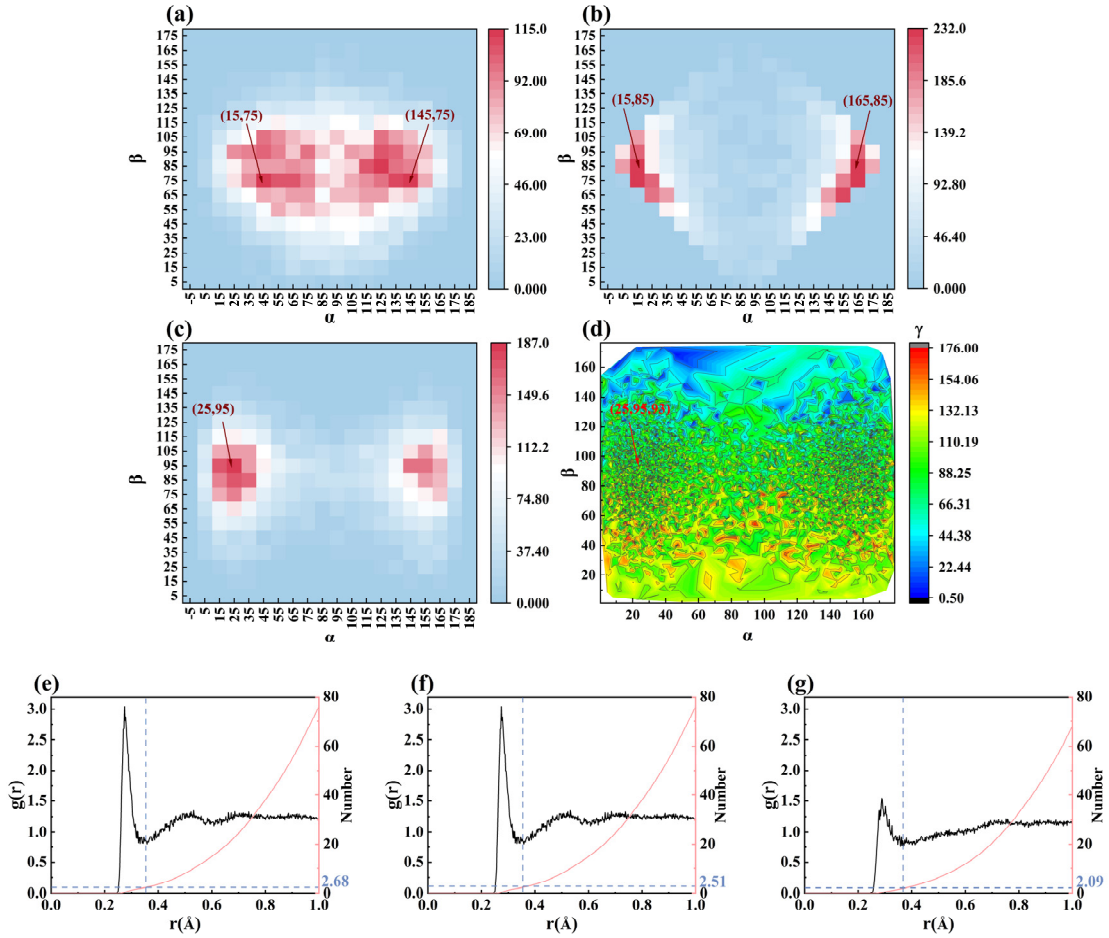

Fig. S4 Angle (α, β, γ) distribution probability of **(a)** Ph, **(b)** 4-HBA, or **(c)** VL with respect to A-W interface; radial distribution function (RDF) and the coordination number *N* of **(e)** $H_{Ph\text{-}OH}\text{-}O_{H_2O}$, **(f)** $H_{4\text{-}HBA\text{-}OH}\text{-}O_{H_2O}$, and **(g)** $H_{VL\text{-}OH}\text{-}O_{H_2O}$ at the A-W interface.

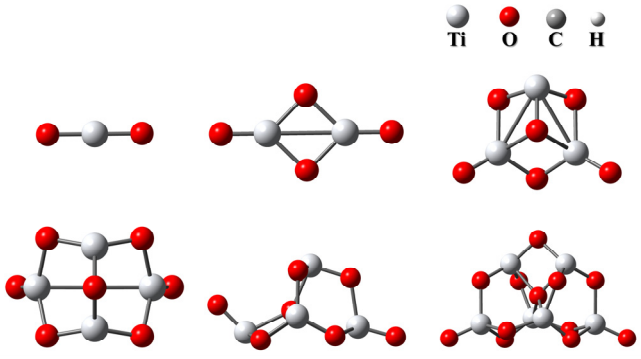

Fig. S5 The minimum energy structures of $(TiO_2)_n$ (n = 1–6) obtained at the M06-2X/6-31 + g(d,p)/LANL2DZ level.

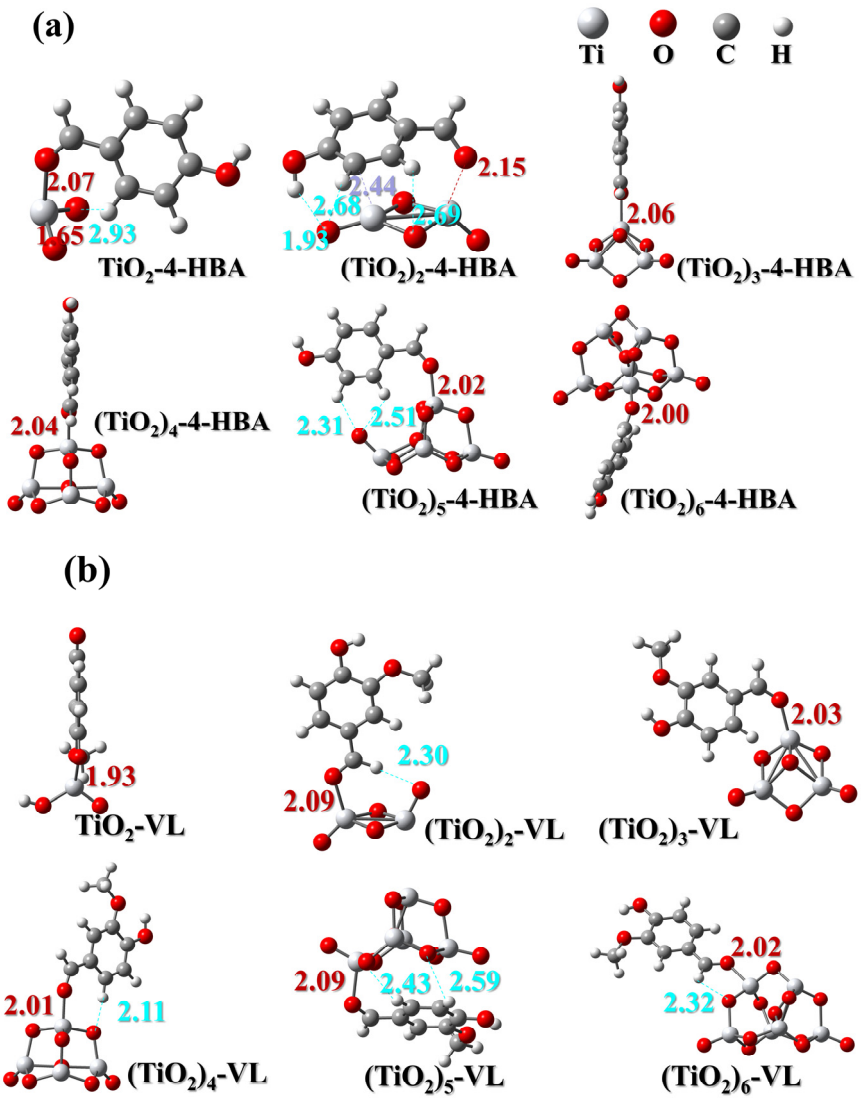

Fig. S6 The minimum energy structures of six $(TiO_2)_n$ (n = 1–6) obtained at the M06-2X / 6-31 + g(d,p) / LANL2DZ level.

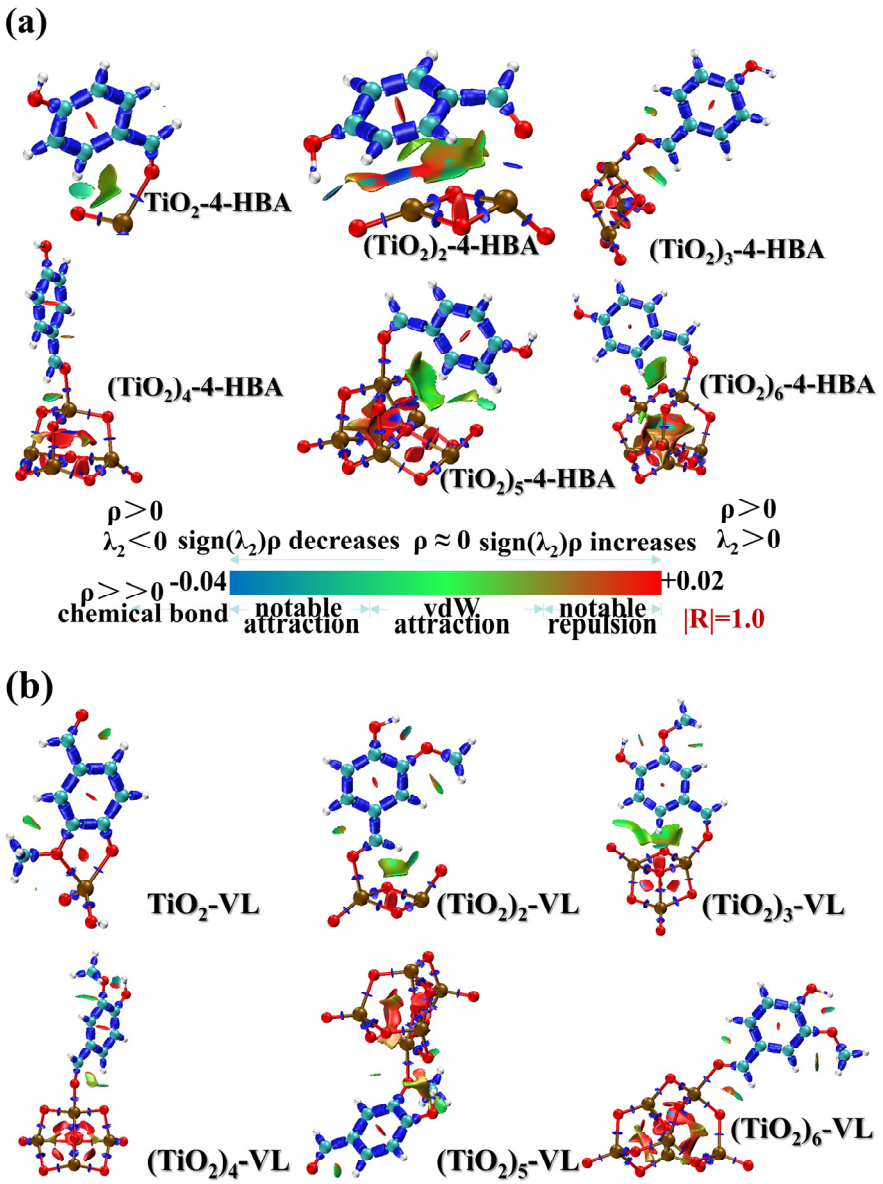

Fig. S7 Interaction region indicator (IRI) analyses of **(a)** 4-HBA and **(b)** VL on $(TiO_2)_n$ (n = 1 – 6) surface.

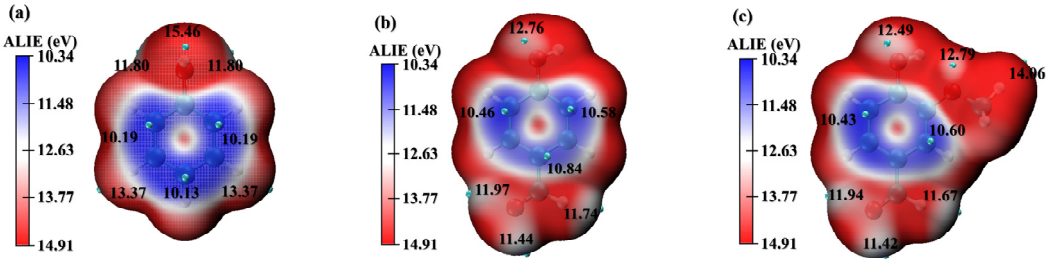

Fig. S8 The average local ionization energy (ALIE) of Ph, 4-HBA, and VL.

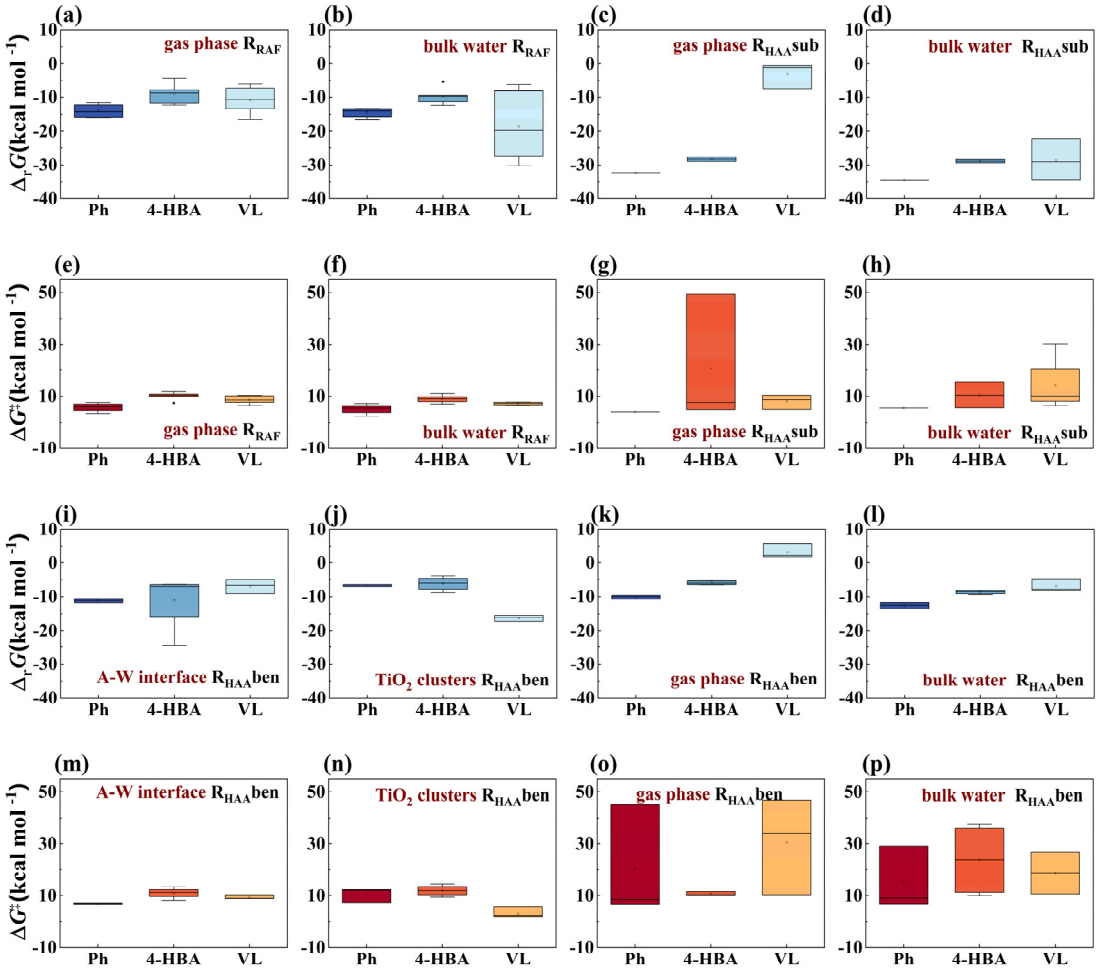

Fig. S9 Statistical charts of calculated **(a)** – **(d)** $\Delta_r G$ and **(e)** – **(h)** $\Delta G^{\ddagger}$ values for O_3-initiated reactions; **(i)** – **(l)** $\Delta_r G$ and **(m)** – **(p)** $\Delta G^{\ddagger}$ values for $HO^{\bullet}$ -initiated reactions.

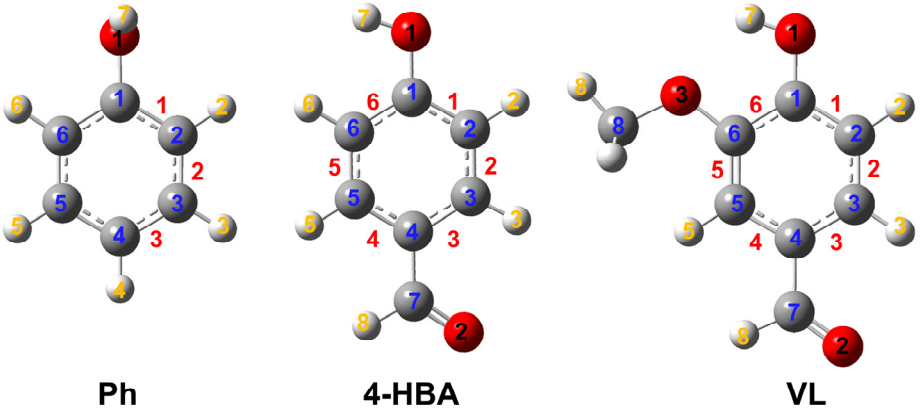

Fig. S10 Minimum free energy structures of the Ph/4-HBA/VL at the SMD/M06-2X/6-31+*G*(d,p) level of theory.

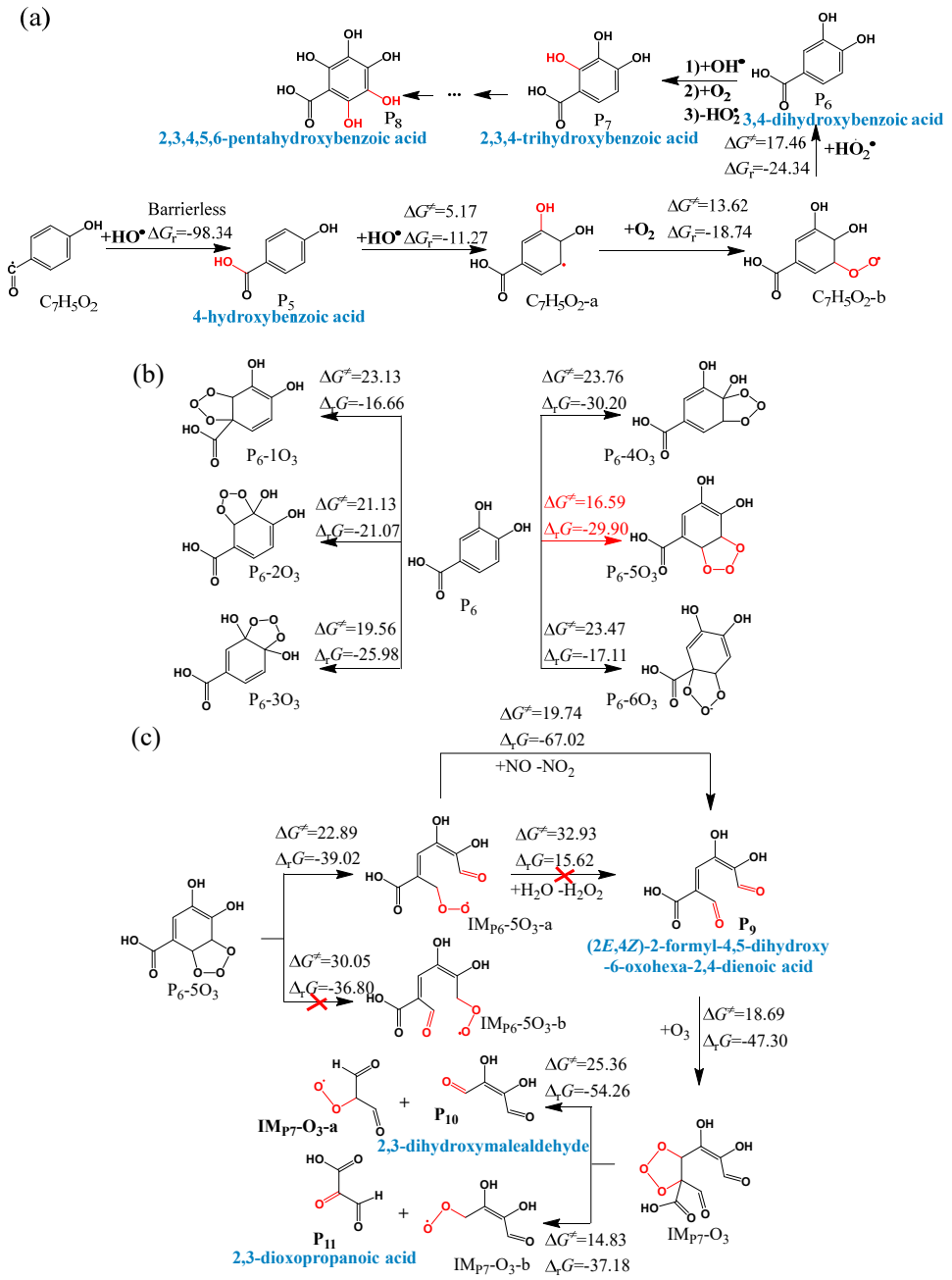

Fig. S11 The subsequent reaction mechanisms of important intermediates (IMs) at A-W interface. Unit in kcal mol $^{-1}$ (Continue on the next page).

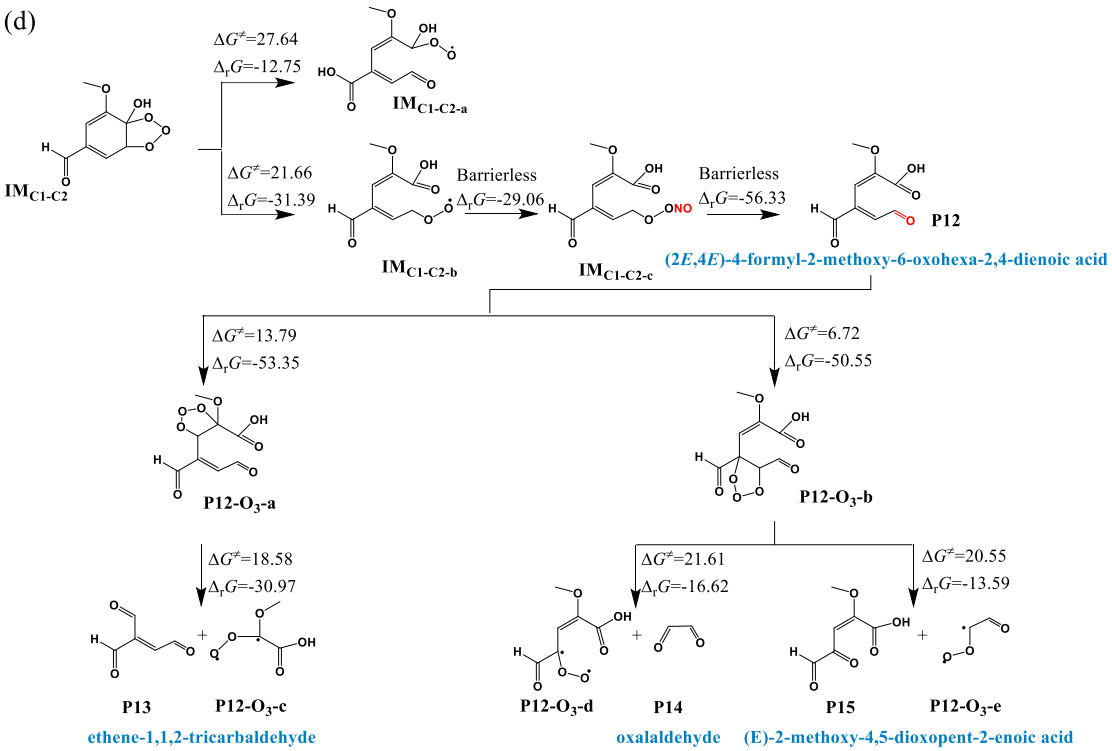

Fig. S11 (Continue) The subsequent reaction mechanisms of important intermediates (IMs) at A-W interface. Unit in kcal mol $^{-1}$.

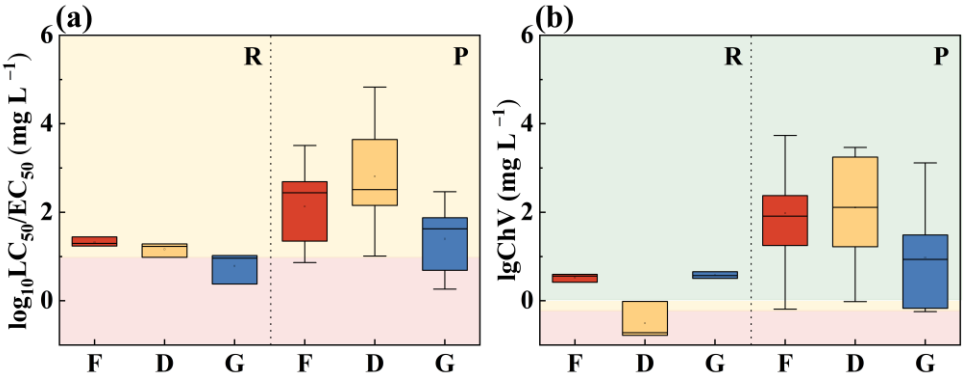

Fig. S12 (a) aquatic acute toxicity and **(b)** chronic toxicity of Ph, 4-HBA, and VL and their oxidation products. F: fish; D: daphnid; G: green algae.

Text S1. The simulation details of umbrella sampling simulations.

For each system, a short relax simulation (2 ns) with the position restraint of the Ph (or 4-HBA or VL) was performed using the NVT ensemble after the completion of the energy minimization. The water molecule with the COM coordinate (2.0 nm, 2.0 nm, 1.5 nm) was chosen as the pull reference group. To obtain the umbrella windows, a 400 ps pull simulation was performed. The Ph (or 4-HBA or VL) molecule was pull towards the COM of the water slab along with z direction at a rate of 0.005 nm ps^{-1} and the pull force constant of 1000 kJ mol^{-1} nm^{-2}. The position of Ph (or 4-HBA, or VL) was restrained in order to on the one hand eliminate the effect of its movement in x and y directions on the reaction coordinate, and on the other hand allow the rotational of the molecule in the pull process. There were 70 windows in the umbrella sampling (US) simulations (Kästner, 2011) and the bound of the R in every window was kept the same as $Z \in [0, 4.0\ nm]$. The distance was varied by steps of 0.05 nm, centered from 4.0 nm to 0 nm.

Text S2. The radial distribution function and coordination number

The radial distribution function (RDF) can be used to estimate the hydrogen bonding (HB) strength between particular atoms. The HB between Ph (4-HBA, or VL) and water at air-water interfaces occurs. The number of water molecules around the Ph (4-HBA, or VL) molecule was obtained by calculating the coordination number (N). Considering the density at the interface is equal to 50% of the nanoparticle interior, the N parameter is obtained as the integrations of g(r) within r=2.5 Å.

Text S3. Details of DFT calculations

The geometry optimizations and harmonic vibrational frequency of all species were determined at the M06–2X/6-31 + G(d,p) level for the gas phase. Intrinsic reaction coordinate calculations (IRCs) were used to confirm each transition state (TS) connecting the reactants (Rs) and products (Ps). The single-point energy calculations were performed at a higher level — M06–2X/6–311++G(3df,2p). The continuum solvation model 'SMD' was used to consider the solvent effect of the bulk water. The reliability of the theoretical level we have chosen has been proved in previous studies (Wang et al., 2021b). The M06-2X/6-31+G(d, p) level for C, O, and H (Yan and Truhlar, 2015; Zhao and Truhlar, 2008a, b) and M06-2X/LANL2DZ level (Hay and Wadt, 1985a; Wadt and Hay, 1985; Hay and Wadt, 1985b) for Ti were used to obtain credible results (An et al., 2021). Fu et al. (Fu et al., 2020) and Wang et al. (Wang et al., 2021a) have used various levels of theory to verify the accuracy of this level. According to previous studies, the LanL2DZ basis set performs well in calculating transition metals (Qu et al., 2018). The geometry optimizations and vibrational frequencies for all reactants (Rs), transition states (TSs), intermediates (IMs), and products (Ps) were obtained. Intrinsic reaction coordinate (IRC) was also used to confirm the correctness of the TSs. Besides, M06-2X/6-311++G(3df,2p)/LANL2TZ (Hay and Wadt, 1985a; Roy et al., 2008) was used to receive single-point energy. At 298 K and 1 atm, Gibbs free energy was obtained. Besides, the free energy corrections also were considered. The adsorption Gibbs free energy was calculated by Eq. (1):

$\Delta G_{ad} = G_{adsorption\ complex} - G_{isolated\ molecule} - G_{surface\ model}$ (1)

Where $\Delta G_{adsorption\ complex}$ is the total energy of the adsorbate-surface complex; $G_{isolated\ molecule}$ is the energy of Ph (or 4-HBA or VL); $G_{surface\ model}$ is the energy of $(TiO_2)_n$ (n = 1-6) clusters.

Text S4. Interaction region indicator (IRI).

$$IRI(\mathbf{r}) = \frac{|\nabla\rho(r)|}{[\rho(r)]^{1.0}} \quad (2)$$

where a is an adjustable parameter, a=1.1 is adopted for standard definition of IRI. IRI is essentially the gradient norm of electron density weighted by scaled electron density. Note that if a=4/3, IRI only differs from RDG by a constant prefactor. Obviously, IRI can be immediately implemented in any code that already supported RDG. As will be shown, by properly choosing isovalue, isosurfaces of IRI are able to exhibit various kinds of interaction regions.

Visual Molecular Dynamics (version 1.9.3) (Humphrey et al., 1996) was used to display the results.

Text S5. Calculation of reaction rate constant.

Chemical reaction process should be considered in the calculation of bimolecular reaction rate constant (k_i) of each elementary reaction (i). The chemical reaction rate constant (k_{chem}) of each reaction route was calculated using conventional transition state theory:

$$k_{chem} = \sigma\kappa\frac{k_B T}{h}K^0 e^{\frac{-\Delta G^{\neq}}{RT}} \quad (3)$$

where k_B and h were the Boltzmann and Planck constants respectively; T was the temperature; R was the gas constant; $\Delta G^{\ddagger}$ was the free energy barrier including the

thermodynamic contribution correction; σ was the reaction path degeneracy, accounting for the number of equivalent reaction paths.

Our calculated the reaction rate constants for the ozonolysis of Ph is 5.27×10^{-20} cm^3 $molecule^{-1}$ s^{-1} which is less than one order of magnitude different from the reaction rate constants for the ozonolysis of guaiacol. Therefore, our results are reliable.

Text S6. Interfacial adsorption properties

To identify the ability of the interface to adsorb gaseous phenolic compounds (Ph, 4-HBA, or VL), the free energy difference from gaseous phenolic compounds (Ph, 4-HBA, or VL) to the interface is defined as: $\Delta G_{gas \rightarrow interface} = G_{interface} - G_{gas}$, where $G_{interface}$ refers to the minimum value at the interface and G_{gas} is the maximum value in the gas phase. The corresponding value reflects whether the interface prefers to adsorb gaseous phenolic compounds (Ph, 4-HBA, or VL).

Text S7. Interface properties of PhCs

The research focused on understanding the behavior of PhCs at A-W interface. The distribution probability of angle (α, β, γ) for Ph/4-HBA/VL in relation to the A-W interface is shown in **Fig. S4(a)–(d)**. The Z-axis is defined as the axis perpendicular to the interface. The angles are formed between the Z-axis and the benzene ring plane, the phenolic hydroxyl group, and the O–αC bound of Ph, 4-HBA, and VL, respectively, denoted as α, β, and γ. In the Ph-A-W, 4-HBA-A-W, and VL-A-W systems, a broad distribution range is observed, suggesting that PhCs are rather randomly distributed across the interface. However, statistically, the highest

distribution range for α and β falls within 15°–25° (or 145°–165°) and 75°–95°, respectively. This applies to both α and β. In the VL-A-W system, the highest distribution range for α is around 93°. To set up the interface reaction environment for further quantum chemical calculations, the radial distribution function (g(r)) of Ph, 4-HBA, and VL at interfaces was computed and is show in **Fig. S4 (e)–(g)**. These figures also display the radial distribution function (RDF) and the coordination number N of $H_{Ph\text{-}OH}–O_{H_2O}$, $H_{4\text{-}HBA\text{-}OH}–O_{H_2O}$, and $H_{VL\text{-}OH}–O_{H_2O}$ at the A-W interface. Peak intensities are observed in the range of 0.25–0.3 Å for $H_{Ph\text{-}OH}–O_{H_2O}$, $H_{4\text{-}HBA\text{-}OH}–O_{H_2O}$, and $H_{VL\text{-}OH}–O_{H_2O}$, as shown in **Fig. 3(e)–(g)**, respectively.

Text S8. Adsorption of Ph, 4-HBA, and VL by TiO_2 Clusters

The investigation into the structural stability of TiO_2 clusters (Zhai and Wang, 2007; Syzgantseva et al., 2011; Arab et al., 2016) has revealed six distinct types of ($(TiO_2)_n$ (n = 1–6)) clusters as depicted in **Fig. S5**. The structural parameter values computed for TiO_2 clusters using the M06–2X/6-31+G(d,p)/LANL2DZ level align with reported experimental values (Calatayud et al., 2008; Bai et al., 2020). **Fig. 4**, **S6**, and **S7** provide additional insights into the adsorption of PhCs on $(TiO_2)_n$ (n = 1–6) clusters.

In **Fig. S6**, the primary interaction for 4-HBA/VL and TiO_2 clusters occurs between the Ti atom and the $O_{\text{-}CHO}$ atom, with distances ranging from 1.93 and 2.07 Å. TiO_2 clusters have a greater potential to interact with the oxygen atom of the aldehyde group than with the oxygen atom of the phenolic hydroxyl group. **Fig. S8** presents the ALIE surface values for the three PhCs considered. Lower ALIE values indicate

weaker binding of electrons, with darker blue regions signifying the lowest local minimum ALIE levels. ALIE values, in the range of 11.42–11.97 eV, for O_{-CHO} atom are lower than those for O_{-OH} atom (12.49–15.46 eV) or O_{-OCH_3} atom (14.96 eV) due to the electron-accepting nature of the aldehyde group. Therefore, the interaction between the Ti atom and O_{-CHO} atom is stronger than with the O_{-OH} or O_{-OCH_3} atoms.

Text S9. Ecotoxicity assessment

We made predictions about the ecotoxicity of Ph, 4-HBA, and VL to three different trophic levels of aquatic creatures (fish, daphnia, and green algae) in order to better understand how the atmospheric oxidation process affects aquatic organisms, specifically fish, daphnia, and green algae. The acute toxicity of Ph, 4-HBA, and VL to aquatic organisms follows the order indicated in **Fig. S11(a)**, which is "green algae > daphnid > fish." According to the criteria in **Table S7**, the acute toxicity of Ph, 4-HBA, and VL is either "very toxic" or "toxic" for three aquatic organisms at concentrations ranging from 2.40–27.70 mg L^{-1}. The transformation products have a greater average acute toxicity dosage to three aquatic creatures than their parent chemicals did (0.79–1.33 mg L^{-1}), as shown by the fact that the transformation products have a value of 1.40–2.82 mg L^{-1}. On the other hand, the acute toxicity of some products, such as P1 (0.26–1.00 mg L^{-1}) and P10 (0.54 mg L^{-1} to "green algae"), is higher than that of their parent chemicals. On the other hand, **Fig. S11(b)** demonstrates that the sequence of "green algae > fish > daphnid" is the one that has the highest average chronic toxicity. In addition, the longterm toxicity of transformation products is often detrimental, but it is lower than that of the parent

chemicals. On the other hand, the chronic toxicity of P1, P2, P3, and P11 is still "toxic/very toxic" to green algae, fish, and daphnid. Consequently, there remains a concern regarding the potential hazards associated with certain transformation products.

References

An, Z., Li, M., Huo, Y., Jiang, J., Zhou, Y., Jin, Z., Xie, J., Zhan, J., and He, M.: The pH-dependent contributions of radical species during the removal of aromatic acids and bases in light/chlorine systems, Chem. Eng. J., 133493, https://doi.org/10.1016/j.cej.2021.133493, 2021.

Fu, Z., Xie, H.-B., Elm, J., Guo, X., Fu, Z., and Chen, J.: Formation of Low-Volatile Products and Unexpected High Formaldehyde Yield from the Atmospheric Oxidation of Methylsiloxanes, Environ. Sci. Technol., 54, 7136-7145, https://doi.org/10.1021/acs.est.0c01090, 2020.

Hay, P. J. and Wadt, W. R.: Ab initio effective core potentials for molecular calculations. Potentials for K to Au including the outermost core orbitals, J. Chem. Phys., 82, 299-310, https://doi.org/10.1063/1.448975, 1985a.

Hay, P. J. and Wadt, W. R.: Ab initio effective core potentials for molecular calculations. Potentials for the transition metal atoms Sc to Hg., J. Chem. Phys., 82, 270-283, https://doi.org/10.1063/1.448799, 1985b.

Humphrey, W., Dalke, A., and Schulten, K.: VMD: Visual molecular dynamics, J Mol Graph Model, 14, 33-38, https://doi.org/10.1016/0263-7855(96)00018-5, 1996.

Kästner, J.: Umbrella sampling, Wires Comput Mol Sci, 1, 932-942, https://doi.org/10.1002/wcms.66, 2011.

Qu, R., Li, C., Liu, J., Xiao, R., Pan, X., Zeng, X., Wang, Z., and Wu, J.: Hydroxyl Radical Based Photocatalytic Degradation of Halogenated Organic Contaminants and Paraffin on Silica Gel, Environ. Sci. Technol., 52, 7220-7229, https://doi.org/10.1021/acs.est.8b00499, 2018.

Roy, L. E., Hay, P. J., and Martin, R. L.: Revised Basis Sets for the LANL Effective

Core Potentials, J. Chem. Theory Comput., 4, 1029-1031, https://doi.org/10.1021/ct8000409, 2008.

Wadt, W. R. and Hay, P. J.: Ab initio effective core potentials for molecular calculations. Potentials for main group elements Na to Bi, J. Chem. Phys., 82, 282-298, https://doi.org/10.1063/1.448800, 1985.

Wang, X., Wei, Y., Zhang, H., Bao, L., He, M., and Yuan, S.: Understanding the properties of methyl vinyl ketone and methacrolein at the air-water interface: Adsorption, heterogeneous reaction and environmental impact analysis, Chemosphere, 283, 131183, https://doi.org/10.1016/j.chemosphere.2021.131183, 2021a.

Wang, X., Liu, S., Bao, L., Zhang, H., Yuan, S., He, M., and Yuan, S.: Enhanced uptake of methacrolein at the acidic nanoparticle interface: Adsorption, heterogeneous reaction and impact for the secondary organic aerosol formation, Sci Total Environ, 800, 149532, https://doi.org/10.1016/j.scitotenv.2021.149532, 2021b.

Yan, Z. and Truhlar, D. G.: The M06 suite of density functionals for main group thermochemistry, thermochemical kinetics, noncovalent interactions, excited states, and transition elements: Two new functionals and systematic testing of four M06 functionals and 12 other functionals (Th, https://doi.org/10.1007/s00214-007-0310-x, 2015.

Zhao, Y. and Truhlar, D. G.: The M06 suite of density functionals for main group thermochemistry, thermochemical kinetics, noncovalent interactions, excited states, and transition elements: two new functionals and systematic testing of four M06-class functionals and 12 other functionals, Theor. Chem. Acc., 120, 215-241, https://doi.org/10.1007/s00214-007-0310-x, 2008a.

Zhao, Y. and Truhlar, D. G.: The M06 suite of density functionals for main group thermochemistry, thermochemical kinetics, noncovalent interactions, excited states, and transition elements: two new functionals and systematic testing of four M06 functionals and 12 other functionals, Theor. Chem. Acc., 119, 525-525, https://doi.org/10.1007/s00214-007-0401-8, 2008b.